

SmCo₅/Fe nanocomposites synthesized from reductive annealing of oxide nanoparticles

Yanglong Hou and Shouheng Sun^{a)}

Department of Chemistry, Brown University, Providence, Rhode Island 02912, USA

Chuanbing Rong and J. Ping Liu

Department of Physics, University of Texas at Arlington, Arlington, Texas 76019, USA

(Received 15 August 2007; accepted 24 September 2007; published online 12 October 2007)

Hard magnetic nanocomposites SmCo₅/Fe_x ($x=0-2.9$) are synthesized by a simultaneous calcium reduction of Sm–Co–O and Fe₃O₄ nanoparticles. The composites consist of nanostructured SmCo₅ and Fe with their average grain sizes at 29 and 8 nm, respectively. The magnetic properties of the composites can be tuned by controlling Fe composition. SmCo₅/Fe_{1.5} shows an enhanced remanent magnetization at 56 emu/g (45 emu/g for SmCo₅). The largest coercivity value of 11.6 kOe is achieved with SmCo₅/Fe_{0.23}. The synthesis represents a general process toward SmCo-based exchange-spring nanocomposites for high performance permanent magnet applications. © 2007 American Institute of Physics. [DOI: 10.1063/1.2799170]

Nanocomposites containing exchange-coupled magnetically hard and soft phases are desirable for permanent magnet applications.¹⁻¹⁰ The intimate contact between the hard and soft phases renders the composites large coercivity, high magnetization, and enhanced energy product. To preserve the coercivity in the isotropic two-phase systems, the size of the soft magnetic grains should be of the order of 10 nm.¹⁻⁶ SmCo₅/Fe exchange-coupled nanocomposites represent an important class of high performance permanent magnetic materials with SmCo₅ offering large coercivity, high Curie temperature, and Fe providing high magnetic moment.¹¹⁻¹⁵ Such composites are normally made by physical methods, such as mechanical milling and sputtering.¹⁶⁻²⁰ Although the compositions of the composites are well controlled in these physical processes, the fabrications are either not reliable for making composites with the grain sizes in nanometer region, or have difficulties in producing large quantity of composites for applications as bulk nanocomposite magnets.

Here, we report that a simple chemical approach can be used to make SmCo₅/Fe nanocomposites with controlled coercivity and enhanced magnetization. The synthesis is based on the precipitation of Sm and Co salts from their aqueous solutions with a base in the presence of monodisperse Fe₃O₄ nanoparticles. The Fe₃O₄ nanoparticles are embedded in SmCo-hydroxide matrix and the composites are annealed at high temperature in the presence of a strong reducing agent (Ca) and a dispersion medium KCl. The high temperature reductive annealing converts Fe₃O₄ into Fe and SmCoO into SmCo. The Sm–Co–O or Sm–Co acts as protecting matrix to prevent Fe nanoparticles from growing into large single crystals. The nanocomposites consist of a hcp structured SmCo₅ and α -Fe with the average grain sizes at 29 and 8 nm, respectively. SmCo₅ and Fe form exchange-coupled nanocomposites with both coercivity and magnetization dependent on doping percentage of Fe. At room temperature, the SmCo₅/Fe_{1.5} shows a H_c of 6.05 kOe (8.8 kOe for SmCo₅) and an enhanced remanent magnetization at 56 emu/g (45 emu/g for SmCo₅), and the SmCo₅/Fe_{0.23} have the largest coercivity at 11.6 kOe.

To embed monodisperse Fe₃O₄ nanoparticles into the Sm–Co–O matrix, the hydrophobic Fe₃O₄ nanoparticles synthesized according to a previous publication²¹ were converted into hydrophilic ones by replacing the oleate and oleylamine with tetrabutyl ammonium hydroxide (Bu₄NOH) following a procedure reported on surface modification of FePt nanoparticles.²² The hydrophilic Fe₃O₄ nanoparticles were then mixed with the aqueous solutions of SmCl₃ and CoCl₂ and were further precipitated out along with SmCo-hydroxide by adding the aqueous Bu₄NOH to the mixture solution. The precipitate was then baked at 120 °C to convert the hydroxide into oxide and to embed the Fe₃O₄ nanoparticles into the Sm–Co-oxide matrix. The molar ratio of Sm/Co/Fe was controlled by the mass ratio of the precursor salts and Fe₃O₄ nanoparticles. These composite nanoparticles can be used as starting precursor to make SmCo₅/Fe nanocomposites.

The reductive annealing was performed in the presence of metallic calcium (Ca) and at high temperature >800 °C. The composite nanomaterials were mixed with KCl and metal Ca. KCl (mp=770 °C) was used as a dispersion medium for the reactants to facilitate the complete reduction of Sm–Co–O and Fe₃O₄, and to prevent SmCo₅ or Fe from growing into large crystals in the high temperature annealing conditions. Among various annealing temperatures and times tested, 900 °C for 1 h was found to be the optimum annealing condition to convert Sm–Co–O–Fe₃O₄ into SmCo₅/Fe_x. The Sm/Co/Fe composition in the nanocomposites was analyzed by energy-disperse x-ray spectroscopy and inductively coupled plasma-atomic emission spectroscopy. SmCo₅ was obtained from the 1/4 Sm/Co-salt mixture while the Fe fraction was carried over from the starting materials to the final product and, therefore, was readily tuned from $x=0-2.9$.

Figure 1 shows the x-ray diffraction (XRD) patterns of the SmCo₅/Fe_x composites prepared from the reductive annealing. The crystal structure of the Sm–Co can be indexed with the standard SmCo₅ pattern,²³ indicating that high temperature reduction and interface diffusion lead to the formation of hcp structured SmCo₅ when $x<0.44$. When Fe was doped into SmCo₅ structure, it is likely that Fe diffuses into the SmCo₅ phase, as confirmed by the increase of lattice

^{a)}Electronic mail: ssun@brown.edu

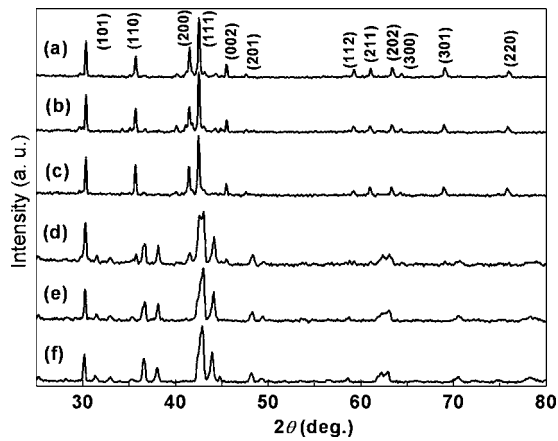


FIG. 1. XRD patterns (Cu $K\alpha$ radiation at $\lambda=1.5418 \text{ \AA}$) of $\text{SmCo}_5/\text{Fe}_x$ composites with (a) $x=0$, (b) $x=0.23$, (c) $x=0.44$, (d) $x=1.0$, (e) $x=1.5$, and (f) $x=2.9$.

parameter from $a=0.49980 \text{ nm}$ and $c=0.3965 \text{ nm}$ for $x=0$ to $a=0.50080 \text{ nm}$ and $c=0.39715 \text{ nm}$ for $x=0.44$. When the Fe content x is higher than 1.0, a rhombohedral $\text{Sm}_2\text{Co}_{17}$ phase might also be present, as indicated by peaks at 36° and 38° . The single phased Fe is difficult to characterize in these diffraction patterns as its major (110) peak overlaps with the peak in $\text{Sm}_2\text{Co}_{17}$ phase. The correlated SmCo_5 crystal size estimated from the (101) diffraction peak using Scherrer's formula is 29 nm.

The nanocrystalline feature of both SmCo_5 and Fe in the composites is characterized with transmission electron microscopy (TEM). Figure 2(a) is the dark field TEM image of the $\text{SmCo}_5/\text{Fe}_1$ nanocomposites. It was obtained from the (110) diffraction beam of the Fe particles in the composites, as shown in the selected area electron diffraction (SAED) pattern in the inset of Fig. 2(a). The bright dots with an average size of 8 nm represent Fe nanoparticles. The ring pattern in the inset is a characteristic of the three-dimensional random orientation of both SmCo_5 and Fe nanograins within the composite structure. The high resolution TEM (HRTEM) image of a typical $\text{SmCo}_5/\text{Fe}_1$ aggregate is shown in Fig. 2(b). It can be seen that the sample consists of two different nanoscale domains, one with lattice fringe distance at 0.29 nm and another at 0.20 nm, corresponding to the (101) planes (interplane distance at 0.291 nm) in the hcp structured SmCo_5 and the (110) planes (interplane distance at 0.201 nm) in bcc-Fe.

Magnetic hysteresis measurements prove that $\text{SmCo}_5/\text{Fe}_x$ ($x=0-2.9$) nanocomposites are ferromagnetic at

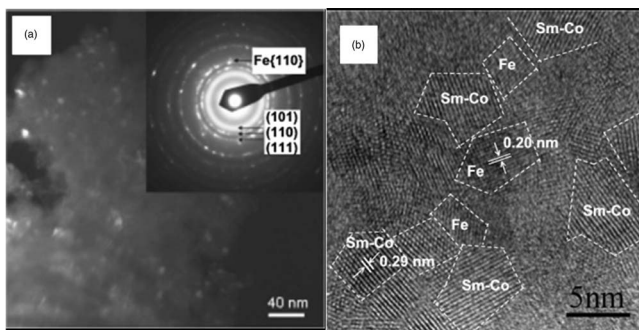


FIG. 2. (a) Dark field TEM image of the $\text{SmCo}_5/\text{Fe}_1$ nanocomposites. Inset: SAED of the nanocomposites. (b) HRTEM image of a single aggregate of the $\text{SmCo}_5/\text{Fe}_1$ nanocomposites with the dashed lines circling the nanocrystalline grains of either SmCo_5 or Fe.

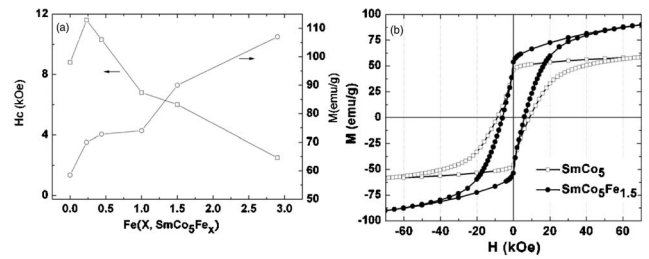


FIG. 3. (a) Change in coercivity and magnetic moment with Fe composition in the $\text{SmCo}_5/\text{Fe}_x$ nanocomposites. (b) Hysteresis loops of the nanocomposites SmCo_5 and $\text{SmCo}_5/\text{Fe}_{1.5}$ at room temperature.

room temperature. Incorporation of Fe particles into the SmCo_5 structure changes both coercivity (H_c) and magnetization of the composites. This can be readily seen in Fig. 3(a), where measured coercivity values and saturation magnetization (M_s) of the SmCo_5Fe_x composites depend on x . Here, the M_s values were approximated from the magnetization curves measured under 7 T. It shows that an addition of a small amount of Fe increases the coercivity to the maximum of 11.6 kOe at $x=0.23$. This is likely caused by the fact that the original Co content may be slightly lower than the nominal composition of 1:5 and the diffusion of Fe into SmCo_5 lattice occurs. Further increase of Fe content leads to either more diffusion or the formation of Fe grains and thus, the nearly monotonous decrease in coercivity and increase in magnetization. Figure 3(b) shows the representative hysteresis loops of SmCo_5 and $\text{SmCo}_5/\text{Fe}_{1.5}$ nanocomposites. It can be seen that the loop from the $\text{SmCo}_5/\text{Fe}_{1.5}$ composites has a high remanent magnetization (M_r) compared to that from the SmCo_5 . This confirms that incorporation of the nanometer soft magnetic Fe phase into the hard SmCo_5 matrix can indeed achieve enhanced magnetization. Furthermore, all the hysteresis loops of the nanocomposites show single phase behaviors without any observable kinks. The remanence ratios of the hysteresis loops are larger than the value of 0.5 predicted for randomly oriented, noninteracting Stoner-Wohlfarth particles.²⁴ This further indicates the strong intergrain exchange coupling in the nanocrystalline $\text{SmCo}_5/\text{Fe}_x$ magnets.

The exchange-coupled two-phase structure can be characterized by the recoil measurements of the nanocomposites. Figure 4(a) is the recoil loops of the $\text{SmCo}_5/\text{Fe}_1$ nanocomposites. It contains a series of slightly open and fairly steep minor loops, which implies a two-phase structure in the composites.²⁵ The $\delta M-H$ measurements are used to verify the nature of the exchange coupling between the SmCo_5 and Fe phases.²⁶ δM is defined as $M_d(1-2M_r)$, where M_d is the

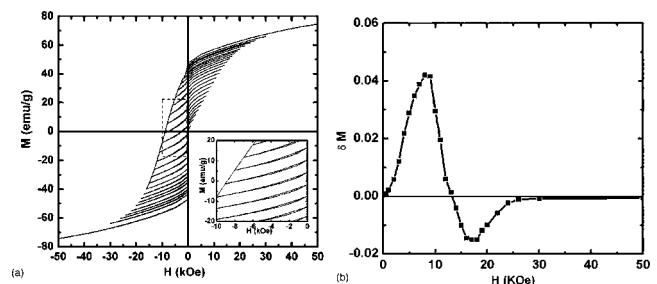


FIG. 4. (a) Recoil loops of the nanocomposite $\text{SmCo}_5/\text{Fe}_1$. The loops were obtained by starting from a point in demagnetization curve to a remanent point with the field decreasing to zero and then back to the starting point. (b) $\delta M-H$ plot of the nanocomposite $\text{SmCo}_5/\text{Fe}_1$.

reduced dc demagnetization remanence curve and M_r is the reduced isothermal remanence curve. For nanocrystalline single-phase magnets, δM always has high positive values, indicating an exchange type of interactions.^{27,28} These interactions suddenly drop to zero or small negative values during reversal as a result of the cooperative switching of the exchange-coupled grains. Figure 4(b) is the δM plot of the composite $\text{SmCo}_5/\text{Fe}_1$ sample. In this composite, δM is initially positive due to the existence of exchange coupling, but it becomes negative after the reversal, suggesting magnetostatic interactions in the composite due to the presence of soft magnetic Fe phase. This observation is a further evidence for the two-phase exchange coupling in the composite, similar to what has been reported in a ball-milled nanocomposite magnet where a soft phase causes negative δM value.²⁹

In summary, hard magnetic exchange-spring nanocomposites $\text{SmCo}_5/\text{Fe}_x$ ($x=0-2.9$) have been synthesized by a facile calcium reduction of the mixture of Sm-Co-O and Fe_3O_4 nanoparticles. The composites contain a hcp structured SmCo_5 with an average grain size of 29 nm and metallic Fe at 8 nm. The $\text{SmCo}_5/\text{Fe}_{1.5}$ shows an enhanced remanent magnetization of 56 emu/g (45 emu/g for SmCo_5) with a H_c at 6.05 kOe (8.8 kOe for SmCo_5). The largest coercivity of 11.6 kOe is achieved with $\text{SmCo}_5/\text{Fe}_{0.23}$. Using similar synthetic strategy, SmCo/CoFe nanocomposites can also be made if CoFe_2O_4 instead of Fe_3O_4 nanoparticles are used in the synthesis. With structure, composition, and nanoscale morphology control, magnetic properties of these nanocomposites can be tuned and the optimized energy product should be obtained. Work on obtaining square hysteresis loop from the nanocomposites for high energy product is underway.

The work was supported by ONR/MURI under Grant No. N00014-05-1-0497.

¹E. F. Kneller and R. Hawig, IEEE Trans. Magn. **27**, 3588 (1991).

²R. Skomski and J. M. D. Coey, Phys. Rev. B **48**, 15812 (1993).

³T. Schrefl, H. Kronmüller, and J. Fidler, J. Magn. Magn. Mater. **127**, L273 (1993).

⁴Z. J. Guo, J. S. Jiang, J. E. Pearson, S. D. Bader, and J. P. Liu, Appl. Phys. Lett. **81**, 2029 (2002).

⁵Z. S. Shan, J. P. Liu, V. M. Chkka, H. Zeng, and J. S. Jiang, IEEE Trans. Magn. **38**, 2907 (2002).

⁶C. B. Rong, H. W. Zhang, R. J. Chen, S. L. He, and B. G. Shen, J. Magn. Magn. Mater. **302**, 126 (2006).

⁷W. C. Chang, D. Y. Chiou, S. H. Wu, B. M. Ma, and C. O. Bounds, Appl. Phys. Lett. **72**, 121 (1998).

⁸K. Barmak, J. Kim, R. A. Ristau, and L. H. Lewis, IEEE Trans. Magn. **38**, 2799 (2002).

⁹H. Zeng, J. Li, J. P. Liu, Z. L. Wang, and S. Sun, Nature (London) **420**, 395 (2002).

¹⁰J. S. Jiang, J. E. Pearson, Z. Y. Liu, B. Kabius, S. Trasobares, D. J. Miller, S. D. Bader, D. R. Lee, D. Haskel, G. Srajer, and J. P. Liu, J. Appl. Phys. **97**, 10K311 (2005).

¹¹R. F. Sabiryanov and S. S. Jaswal, Phys. Rev. B **58**, 12071 (1998).

¹²Z. D. Zhang, W. Liu, J. P. Liu, and D. J. Sellmyer, J. Phys. D **33**, R217 (2000).

¹³I. A. Al-Omari, R. Skomski, R. A. Thomas, D. Leslie-Pelecky, and D. J. Sellmyer, IEEE Trans. Magn. **37**, 2534 (2001).

¹⁴A. V. Khvalkovskii, K. A. Zvezdin, A. A. Zvezdin, V. S. Gornakov, D. G. Skachkov, and P. Perlo, Physica B **372**, 358 (2006).

¹⁵Y. Choi, J. S. Jiang, Y. Ding, R. A. Rosenberg, J. E. Pearson, S. D. Bader, A. Zambano, M. Murakami, I. Takeuchi, Z. L. Wang, and J. P. Liu, Phys. Rev. B **75**, 104432 (2007).

¹⁶Y. N. Liu, M. P. Dallimore, P. G. McCormick, and T. Alonso, J. Magn. Magn. Mater. **116**, L320 (1992).

¹⁷S. K. Chen, J. L. Tsai, and T. S. Chin, J. Appl. Phys. **79**, 5964 (1996).

¹⁸J. Zhang, S. Y. Zhang, H. W. Zhang, B. G. Shen, and B. H. Li, J. Appl. Phys. **89**, 2857 (2001).

¹⁹J. S. Jiang and S. D. Bader, Scr. Mater. **47**, 563 (2002).

²⁰V. Neu, K. Hafner, A. K. Patra, and L. Schltz, J. Phys. D **39**, 5116 (2006).

²¹Z. Xu, Y. Hou, and S. Sun, J. Am. Chem. Soc. **129**, 8698 (2007).

²²V. Salgueiriño-Maceira, L. M. Liz-Marzán, and M. Farle, Langmuir **20**, 6946 (2004).

²³JCPDS Card No. 65-8981.

²⁴A. Stancu and C. Păpusoi, IEEE Trans. Magn. **30**, 4308 (1994).

²⁵C. B. Rong, V. Nandwana, N. Poudyal, Y. Li, J. P. Liu, Y. Ding, and Z. L. Wang, J. Phys. D **40**, 712 (2007).

²⁶P. E. Kelly, K. O'Grady, P. I. Mayo, and R. W. Chantrell, IEEE Trans. Magn. **25**, 3881 (1989).

²⁷H. Zeng, S. Sun, T. S. Vedantam, J. P. Liu, Z. R. Dai, and Z. L. Wang, Appl. Phys. Lett. **80**, 2583 (2002).

²⁸C. B. Rong, H. W. Zhang, B. G. Shen, and J. P. Liu, Appl. Phys. Lett. **88**, 42504 (2006).

²⁹A. Bollero, O. Gutfleisch, K.-H. Müller, and L. Schultz, J. Appl. Phys. **91**, 8159 (2002).